ADVANCED FUNCTIONAL MATERIALS
www.afm-journal.de

Transient Support from Fibroblasts is Sufficient to Drive Functional Vascularization in Engineered Tissues

*Hyun-Ho Greco Song, Alex Lammers, Subramanian Sundaram, Logan Rubio, Amanda X. Chen, Linqing Li, Jeroen Eyckmans, Sangeeta N. Bhatia, and Christopher S. Chen**

Formation of capillary blood vasculature is a critical requirement for native as well as engineered organs and can be induced in vitro by coculturing endothelial cells with fibroblasts. However, whether these fibroblasts are required only in the initial morphogenesis of endothelial cells or needed throughout is unknown, and the ability to remove these stromal cells after assembly can be useful for clinical translation. In this study, a technique termed CAMEO (Controlled Apoptosis in Multicellular Tissues for Engineered Organogenesis) is introduced, whereby fibroblasts are selectively ablated on demand, and it is utilized to probe the dispensability of fibroblasts in vascular morphogenesis. The presence of fibroblasts is shown to be necessary only during the first few days of endothelial cell morphogenesis, after which they can be ablated without significantly affecting the structural and functional features of the developed vasculature. Furthermore, the use of CAMEO to vascularize a construct containing primary human hepatocytes that improved tissue function is demonstrated. In conclusion, this study suggests that transient, initial support from fibroblasts is sufficient to drive vascular morphogenesis in engineered tissues, and this strategy of engineering-via-elimination may provide a new general approach for achieving desired functions and cell compositions in engineered organs.

1. Introduction

Establishing new capillary beds is critical for supporting the metabolic demands and overall health of tissues and organs. This occurs not only in development, but also throughout adult life in both regenerative and disease settings.[1] One mechanism by which such vessel beds form involves the spontaneous assembly of endothelial cells into interconnected networks, and ultimately, perfusable blood vessels.[2,3] Understanding and harnessing this vasculogenesis process for translational applications has been of keen interest.[4,5]

A key observation was that coculture of endothelial cells with fibroblasts could induce endothelial cells to form vascular networks in vitro with minimal additional growth factors and cytokines.[6] In the presence of fibroblasts, endothelial cells spontaneously connected and developed multicellular structures associated with endothelial cell polarization, lumen formation, tubulogenesis, and vessel maturation following a process reminiscent of vasculogenesis.[7–11] Incorporating this process in microfluidic culture systems, it has more recently been shown that vasculogenic networks can integrate and support flow.[12–16]

The exact mechanism by which fibroblasts support vascular morphogenesis is not well understood, but the benefit is even conserved in vivo as incorporation of fibroblasts with endothelial cells in implantable constructs enhances in vivo vascularization.[17–20] The utility of such stromal populations in supporting

H.-H. G. Song, Prof. S.N. Bhatia
Harvard-MIT Program in Health Sciences and Technology
Institute for Medical Engineering and Science
Massachusetts Institute of Technology
Cambridge, MA 02139, USA
H.-H. G. Song, A. Lammers, Dr. S. Sundaram, L. Rubio, Dr. L. Li, Prof. J. Eyckmans, Prof. C. S. Chen
Biological Design Center
Department of Biomedical Engineering
Boston University
Boston, MA 02215, USA
E-mail: chencs@bu.edu
H.-H. G. Song, A. Lammers, Dr. S. Sundaram, Dr. L. Li, Prof. J. Eyckmans, Prof. S.N. Bhatia, Prof. C. S. Chen
Harvard Wyss Institute for Biologically Inspired Engineering
Boston, MA 02115, USA
The ORCID identification number(s) for the author(s) of this article can be found under https://doi.org/10.1002/adfm.202003777.
A. X. Chen
Department of Biological Engineering
Massachusetts Institute of Technology
Cambridge, MA 02139, USA
A. X. Chen, Prof. S. N. Bhatia
David H. Koch Institute for Integrative Cancer Research
Massachusetts Institute of Technology
Cambridge, MA 02142, USA
Prof. S. N. Bhatia
Department of Electrical Engineering and Computer Science
Massachusetts Institute of Technology
Cambridge, MA 02142, USA
Prof. S. N. Bhatia
Howard Hughes Medical Institute
Chevy Chase, MD 20815, USA

DOI: 10.1002/adfm.202003777

cell function extends well beyond effects on endothelial cells, as they have been used in supporting stem cells culture, hepatocyte function, cardiac function, and more.[21–25] Therefore, stromal cells are a convenient, all-in-one population of cells for many coculture systems. However, it remains unclear whether the stromal cells are needed permanently to support these specialized cell functions, and in particular for endothelial cell vasculogenesis, whether they are required only during the initial morphogenetic events.

To address this question, we developed a technique termed CAMEO (Controlled Apoptosis in Multicellular Tissues for Engineered Organogenesis) which allows for a temporal control over the ablation of a select cell population, such as fibroblasts, within a 3D multicellular tissue after a short period of coculture. This technique repurposes the inducible caspase-9 (iCasp9) kill-switch gene that was originally developed as a fail-safe for T-cell therapies.[26–28] By combining CAMEO with our microfluidic vasculogenesis model, we demonstrate that transient, initial support from fibroblasts is sufficient to drive functional neovascularization in engineered tissues. We then apply this insight to engineer vascularized, perfusable liver tissues embedded with human primary hepatocytes. Our approach of "engineering-via-elimination" provides new opportunities for not only studying the time dependencies of cell populations for processes such as vasculogenesis as demonstrated here, but also engineering vasculature in multicellular organ-specific tissues where the presence of fibroblasts may be undesirable.

2. Results and Discussion

2.1. Fibroblasts Enhance Self-Assembly of a Perfused Vasculature in Microfluidic Devices

We first set out to establish a system that enables the 3D morphogenesis of an endothelial cell and fibroblast coculture to result in a self-assembled, perfusable vascular network connected to microfluidic channels. Building on a previously reported device that we originally designed to study angiogenesis in vitro,[29,30] we developed a new iteration that supports vasculogenesis. This new microfluidic device consists of a polydimethylsiloxane (PDMS) silicone-based mold bonded to a glass coverslip that features a central tissue chamber (cells plus extracellular matrix) through which two endothelial cell-lined vessels can be perfused. To achieve this arrangement, briefly, two guides on the side of the PDMS device were designed for the insertion of two parallel needles (300 μm in diameter and 1 mm apart) that traverse the central chamber (**Figure 1**a). Once the needles were inserted, a fibrinogen solution containing human umbilical vein endothelial cells (HUVECs) and growth-arrested human dermal fibroblasts (HDFs) were added into the tissue chamber with thrombin. Once the fibrinogen polymerized into fibrin, the needles were removed to create two hollow, microfluidic channels. These channels were then seeded with additional HUVECs to line the walls in a monolayer. This procedure resulted in the formation of two parallel, endothelialized vessels that could be instantly perfused with media and provide nutrients to the cells in the surrounding extracellular matrix (ECM).

To understand how different densities of fibroblasts would affect the vascular morphogenesis of a given number of endothelial cells, we cocultured HUVECs (3 million cells mL^{-1}) with various concentrations of HDFs (0, 1, 3, and 6 million cells mL^{-1}) for 7 d in the fibrin surrounding the needle-molded endothelial channels (Figure 1b). HUVECs alone were able to make branching networks suggestive of functional vasculature (Figure 1c), but when perfused with a fluorophore-conjugated dextran solution (500 kDa) introduced to one of the microfluidic channels, these structures were unable to transport dextran. Only when HDFs were added to the HUVEC culture did we observe highly branched networks that were able to transport the dextran solution through the self-assembled vessels (Figure 1b,c). Furthermore, cocultures with higher densities of HDFs (3:3 and 3:6 HUVEC:HDF) yielded the highest average percentage of perfused vessels (Figure 1d). While the average diameter of perfused self-assembled vessels (≈45 μm) was similar regardless of the density of HDFs (Figure 1e-i), increasing the density of fibroblasts resulted in a higher density of perfusable vasculature as well as a wider distribution of perfused vessel diameters (Figure 1e-ii). At the highest concentration of HDFs (3:6 ratio), the engineered tissue was well vascularized all throughout its thickness after the 7 d coculture (Figure 1f), which prompted us to use this ratio for the rest of the study.

To visualize the process of vasculogenesis in our microfluidic devices, we seeded green fluorescent protein (GFP)-labeled HUVECs in the needle-molded microfluidic channels to distinguish them from the nonlabeled HUVECs in the bulk fibrin gel. Fixing samples at different times and staining with Ulex Europaeus Agglutinin (UEA) lectin (which labels all HUVECs) allowed us to monitor the process of vascular network formation. As early as day 1, we observed GFP-HUVECs with individual protrusions that started to form intercellular connections (**Figure 2**a). After 3 d in culture, some HUVECs from the microfluidic channels (GFP-labeled) had migrated into the bulk gel and formed chimeric networks with the (unlabeled) HUVECs in the bulk ECM (Figure 2b). Some of these self-assembled structures became perfusable by day 3, and the percentage of perfused vessels continued to increase over time, achieving ≈80% by day 7 (Figure 2c). Interestingly, the average diameters of the perfused vessels in the network remained steady after day 3 (Figure 2d). Together, these data suggest that the vascularization process inside our devices involves both the self-assembly of the bulk HUVECs, and invasion of HUVECs from the microfluidic channels to form a fully interconnected, perfusable vasculature consisting of both the originally templated, larger channels and the self-assembled vasculogenic network.

2.2. CAMEO Allows for a Selective Removal of Fibroblasts from Coculture

To ablate fibroblasts on demand from the developing coculture, we utilized a synthetically engineered, inducible caspase-9 (iCasp9) that was originally developed as a safeguard against acute graft-versus-host disease and rare cytokine release syndrome induced by T-cell therapies to treat cancer.[27,28] Briefly, iCasp9 is a transgene based on human caspase 9 that features a mutated FKBP12 domain (F36V) that can be dimerized with

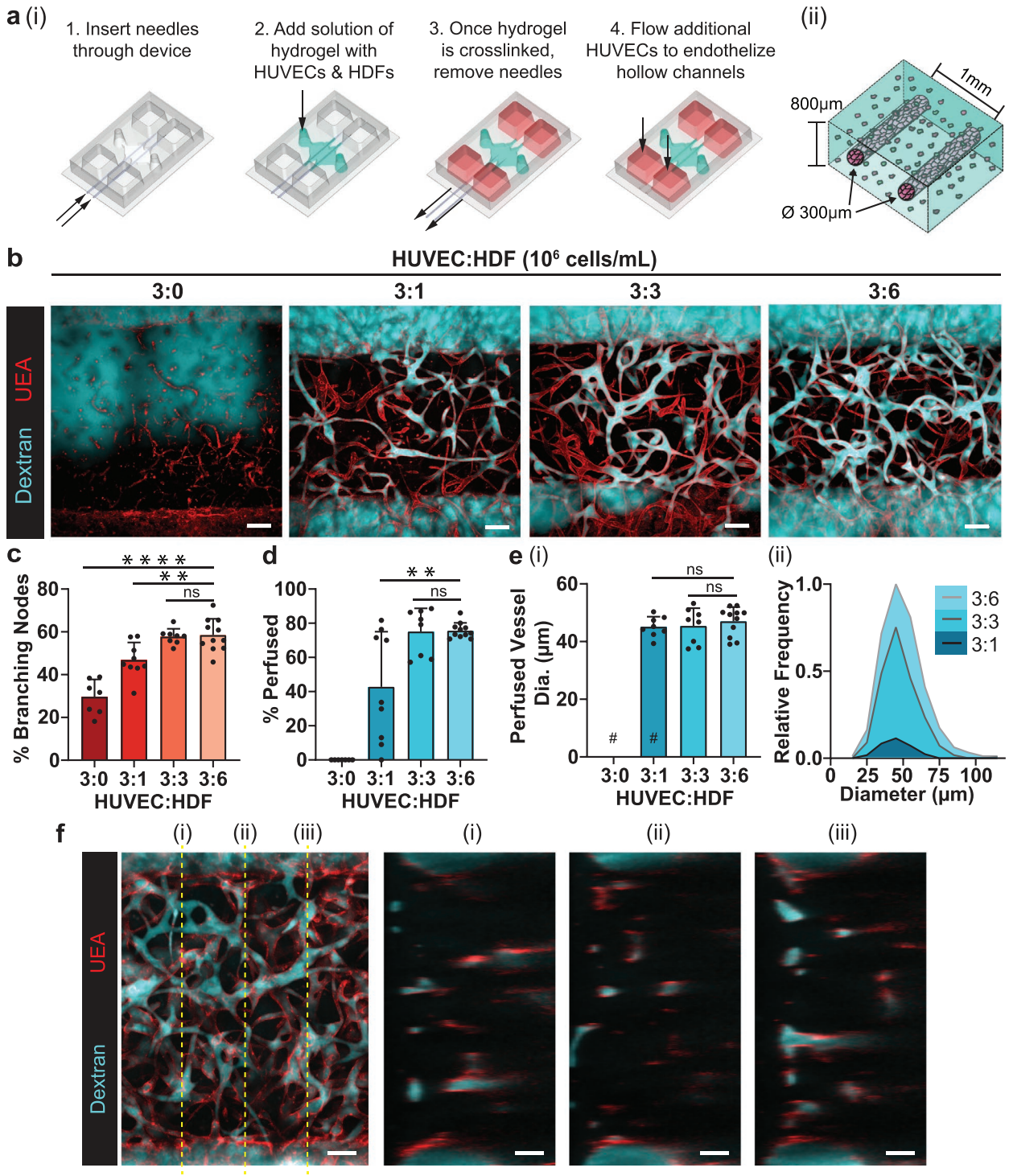

Figure 1. Fibroblasts enhance self-assembly of a perfused vasculature in a 3D microfluidic device. a) Rendering depicting i) the process of seeding the microfluidic device with a fibrin gel containing HUVECs and HDFs cast around two needle-molded, endothelialized microfluidic channels and ii) a close-up illustration of the formed tissue inside the microfluidic device. b) Representative max projections of devices fixed on day 7 with varying HUVEC:HDF ratios. Endothelial networks (red) were perfused with 500 kDa dextran (cyan) through one parent channel to visualize connected luminal networks. c) Quantification of the percentage of branching network nodes from total nodes to evaluate network interconnectedness. Each point represents one device. d) Quantification of the percentage of luminal segments that are perfused to the total segments between the channels. e-i) Quantification of the average diameter of perfused vessel segments for each condition and ii) the individual vessels of each ratio condition summed into bins and normalized to the bin with the greatest count. # represents where data points removed due to no vessels being perfused in those devices. f) Multiphoton max projection of a representative 3:6 ratio device. **: $p < 0.01$; ****: $p < 0.0001$; ns: not significant. Scale bars: b) 150 µm and f) 100 µm.

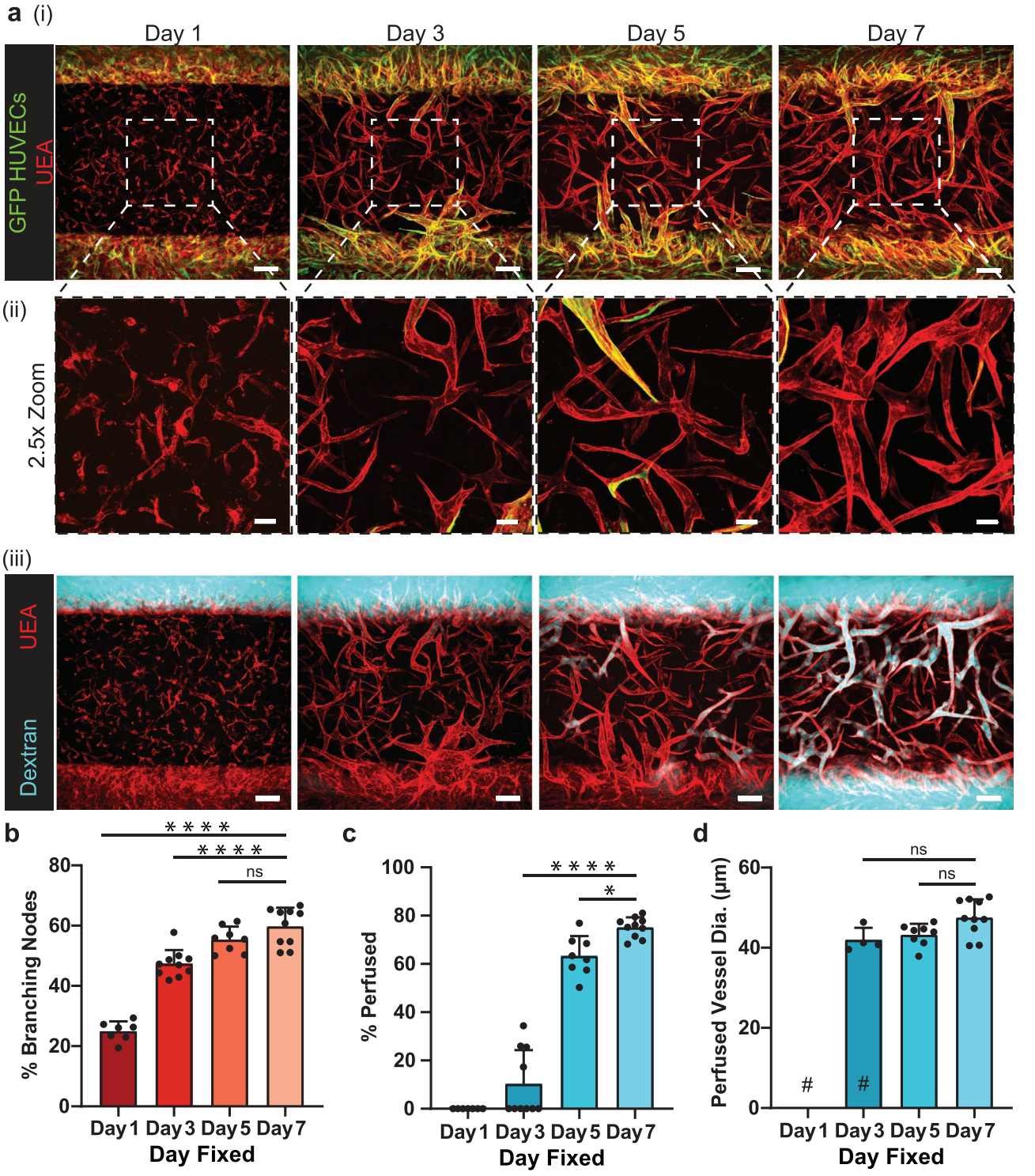

Figure 2. Daily fixations show vasculogenesis formation and functionality. a-i) Representative images of growth progression from multicellular structures to functionally connected vasculature. GFP-expressing HUVECs (green) were seeded in the needle lumen only and eventually complex with the endothelial cells originating in the bulk gel. ii) 2.5× zoomed images of the center of the devices. iii) Same devices shown in (i) with dextran perfusion (cyan) shown along with UEA lectin (red). b) Quantification of percentage of branching nodes, c) percentage of vessels perfused, and d) average diameter of perfused vessels in devices. # represents where data points removed due to no vessels being perfused in those devices. *: $p < 0.05$; ****: $p < 0.0001$; ns: not significant. Scale bars: a-i,iii) 150 μm and a-ii) 50 μm.

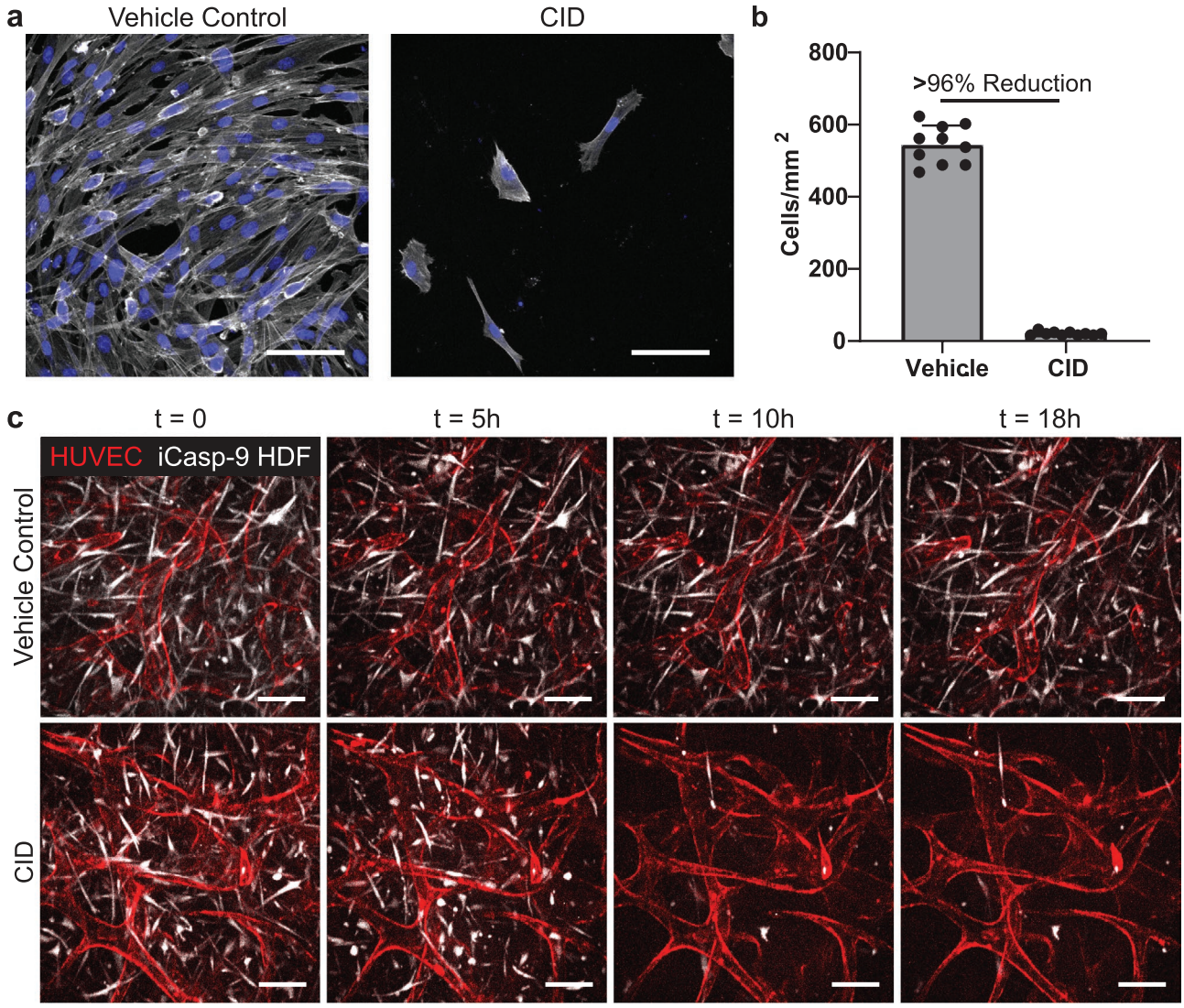

Figure 3. CAMEO allows for a selective removal of fibroblasts from coculture. a) iCasp-HDFs plated on 2D wells, treated with a vehicle control or CID for 24 h, fixed, and imaged. Cells stained with phalloidin (white) and DAPI (blue). b) Quantified cell density of vehicle control- and CID-treated cells. c) Time-lapse images of both device conditions in the microfluidic device. Scale bars: 100 µm.

AP20187, an otherwise inert small molecule chemical inducer of dimerization (CID).[28] Upon dimerization, the iCasp9 proteins become activated, initiating the cascade of caspase-based apoptotic pathways. Since the first description of iCasp9, several clinical studies demonstrated the effectiveness, specificity, and safety of the iCasp9-CID system.[27]

Using this inducible transgene, we established iCasp9-HDFs, and characterized the effectiveness of iCasp9 in these cells. We seeded iCasp9-HDFs on tissue culture plastic, allowed the cells to form a confluent monolayer before adding different concentrations of CID. Even at the lowest concentration of CID used (5×10^{-9} M), the levels of cellular adenosine triphosphate (ATP) dropped precipitously within 2–4 h, suggesting the onset of apoptosis (Figure S1, Supporting Information). In addition, the rapidity of ATP loss increased with increasing CID concentration. Overnight treatment of 10×10^{-9} M CID resulted in an average of ≈96% reduction of iCasp9-HDFs in culture compared to the vehicle control (0.002% ethanol) (**Figure 3**a,b).

To understand whether the ablation of the fibroblasts could induce an inflammatory response in endothelial cells, we cocultured the iCasp9-HDFs with HUVECs, triggered apoptosis with CID, and examined the localization of Nuclear Factor Kappa-light-chain-enhance of activated B cells (NFκB), a TLR-associated marker of the inflammation in HUVECs.[31–33] Whereas the majority of HUVECs treated with 10 ng mL^{-1} TNF-α (positive control) showed nuclear localization of NFκB as early as 4 h and persisted through 48 h post-treatment, we only observed baseline levels similar to vehicle treatment (≈10%) of nuclear NFκB positive HUVECs at 4 h post-CID treatment and undetectable differences at later time points, suggesting that the HUVECs are not activated by the apoptosis of nearby iCasp9-HDFs (Figure S2, Supporting Information).

To examine the temporal and selective control of the iCasp9-HDFs in a 3D system, we cocultured mRuby-LifeAct-HUVECs with iCasp9-HDFs (GFP) in our microfluidic platform. After 7 d of coculture, the cells formed a robust vasculature network as previously observed above, and then we added 10×10^{-9} M of CID (or the vehicle control) to the media. We observed iCasp9-HDFs starting to contract and round up as early as 1 h post-CID addition and the loss of GFP signal (due to photobleaching and the loss of protein production in apoptotic cells) between 5–10 h post-CID addition (Figure 3c and Movie S1, Supporting Information). Interestingly, the rounding event was preceded by a pulse of contraction of the fibroblasts and the surrounding tissue (Movie S1, Supporting Information), consistent with reported caspase-induced ROCK1 activation and ROCK1-mediated actin-myosin contraction.[34,35] Remarkably, we did not observe any immediate, noticeable deterioration of the vascular structure during this massive elimination of HDFs, despite the HUVECs being, in some cases, in direct contact with the dying cells (Figure S3, Supporting Information).

2.3. Transient Coculture with Fibroblasts is Sufficient to Support Vasculogenesis

To understand the dependence of endothelial cells on fibroblasts for vasculogenesis, we cocultured HUVECs with iCasp9-HDFs in our microfluidic devices and ablated the HDFs with CID at different time points (day 0, 1, 3, and 5) during the 7-day culture period (**Figure 4**a). Because a small population of HDFs (≈4%) remain after CID treatment, we growth-arrested the cells with mitomycin C before coculture to prevent their ability to proliferate and repopulate the coculture over this week-long study. When HDFs were ablated within an hour after the completion of the device seeding (day 0), HUVECs were still able to form a network by day 7, but the resulting structure was minimally interconnected (Figure 4b,c), and none of these structures could transport dextran, indicating incomplete vascular morphogenesis similar to HUVEC-only cultures (Figure 4d). Ablating HDFs at day 1 resulted in a few perfusable structures by day 7, but most devices still showed little to no perfusion. Ablating HDFs at day 3 or day 5 yielded highly interconnected and perfusable endothelial networks that were comparable to the control networks in which HDFs were never ablated. The average diameter of the perfused vessels was comparable as well for all conditions except the day 0-deletion condition, although the distribution of the vessel diameters in the day-1-deletion condition was more dispersed. Similar observations were also made with iCasp9-transduced human lung fibroblasts (iCasp9-HLFs) where the HUVECs were able to self-assemble into perfusable vasculature with only 3 d of coculture with iCasp9-HLFs (Figure S4, Supporting Information), suggesting that this short-lived dependency on fibroblast support is not specific to HDFs. All together, these data suggested that the presence of fibroblasts during the first 1–3 d of coculture is critical for the functional vasculogenesis of endothelial cells, but the fibroblasts can be ablated thereafter without structurally affecting the resulting vasculature. With this observation, we termed the technique "Controlled Apoptosis in Multicellular Tissues for Engineered Organogenesis," or CAMEO.

Given that fibroblasts are important effectors of ECM remodeling, we hypothesized that HDFs may support vascular morphogenesis through their early effects on the ECM. To address this hypothesis, we first characterized the stiffness of the tissues during vascular network formation using nanoindentation and assessed the effect of CAMEO on these mechanical properties. Coculturing HUVECs and iCasp9-HDFs for 3 d resulted in tissues with a Young's modulus averaging ≈0.75 kPa, which was substantially stiffer than acellular fibrin gels (≈0.1 kPa) (Figure 4d). Over the next 4 d (days 3–7), these tissues continued to stiffen, reaching an average Young's Modulus of ≈3 kPa at day 7. In contrast, when we induced apoptosis of iCasp9-HDFs at day 3 through CAMEO, the tissues did not further stiffen (≈1 kPa at d7). These data suggest that there is substantial ECM remodeling during culture, and that the changes in ECM are primarily driven by the presence of fibroblasts.

To begin to examine whether HDFs might contribute molecular changes to the ECM during the first days of culture that might support later vascular morphogenesis, we looked to specific ECMs that could be deposited by the fibroblasts. One important matrix protein deposited by fibroblasts during early stages of ECM remodeling is fibronectin, which also has been shown to be important for vascular morphogenesis.[36–38] Therefore, we examined the role of fibronectin in our platform by generating siRNA-mediated fibronectin-knockdown (FN-KD) iCasp9-HDFs and coculturing them with HUVECs in the microfluidic devices for 3 d before CID treatment (Figure 4e). The density of self-assembled endothelial networks was significantly reduced for HUVECs cocultured with the FN-KD iCasp9-HDFs as compared to scrambled siRNA-treated controls. Furthermore, HUVECs cocultured with FN-KD iCasp9-HDFs failed to generate any perfusable vasculature, whereas those cocultured with control iCasp9-HDFs yielded perfusable vasculature (Figure 4f,g), although to a lower extent than previously seen with wild-type HDFs (Figure 1d) likely due to inherent siRNA cytotoxicity in primary cells. Together, this suggests that the continuation of vascular morphogenesis after the ablation of fibroblasts is contingent on provisional ECMs produced by the fibroblasts during the early days of coculture.

2.4. CAMEO Enhances Function of Vascularized, Engineered Hepatic Tissues

Given that fibroblasts are only transiently required for supporting the formation of a functional vasculature, we asked whether CAMEO could be used in the vascularization of tissue constructs with organ-specific parenchymal cells without negatively affecting the function of the parenchymal cells. To investigate this, we employed a tri-culture system consisting of HUVECs, iCasp9-HDFs, and primary human hepatocytes in our microfluidic device. After 5 d of tri-culture, the devices were treated with CID to ablate the iCasp9-HDFs, or with the vehicle control. All samples were fixed at day 7 to evaluate vascular perfusion (**Figure 5**a). In both groups, HUVECs formed perfusable vasculature that permeated the hepatocyte-laden construct (Figure 5b). To evaluate whether the hepatocytes remained functional after CID treatment, levels of albumin and urea, markers for hepatic

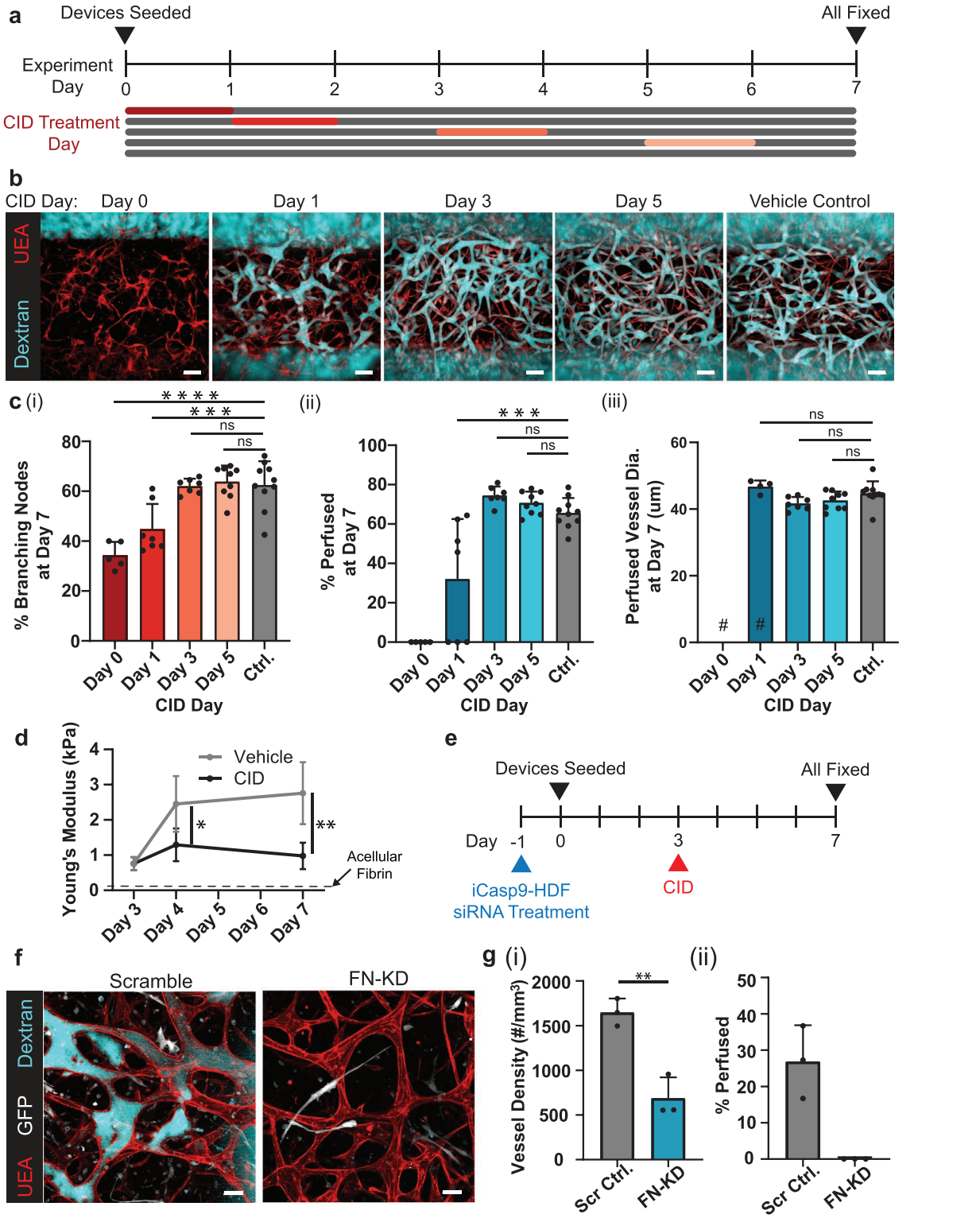

Figure 4. Transient coculture with fibroblasts is enough to drive vascular morphogenesis. a) Experimental timeline. b) Representative max projections of devices treated with CID or vehicle control on a designated day and fixed on day 7. Devices were stained with UEA lectin (red) and perfused with dextran (cyan). c) Quantification of i) percentage of branching nodes, ii) percentage of perfused vessel segments, and iii) average vessel diameter of perfused vessels. # represents where data points removed due to no vessels being perfused in those devices. d) Young's modulus of HUVEC-iCasp9-HDF coculture tissues treated with CID or vehicle at day 3. Dotted line represents the average Young's modulus of acellular fibrin gel at day 3 (≈0.1 kPa). e) Experiment timeline. f) Representative max projection images of dextran-perfusion (cyan), HUVECs (UEA lectin, red) and iCasp9-HDFs and their apoptotic bodies (GFP, white) at day 7. g) Quantification of i) percentage of structures that are perfused with dextran and ii) density of the self-assembled network. *: $p < 0.05$; **: $p < 0.01$; ***: $p < 0.001$; ****: $p < 0.0001$; ns = not significant. Scale bars: b) 150 µm f) 50 µm.

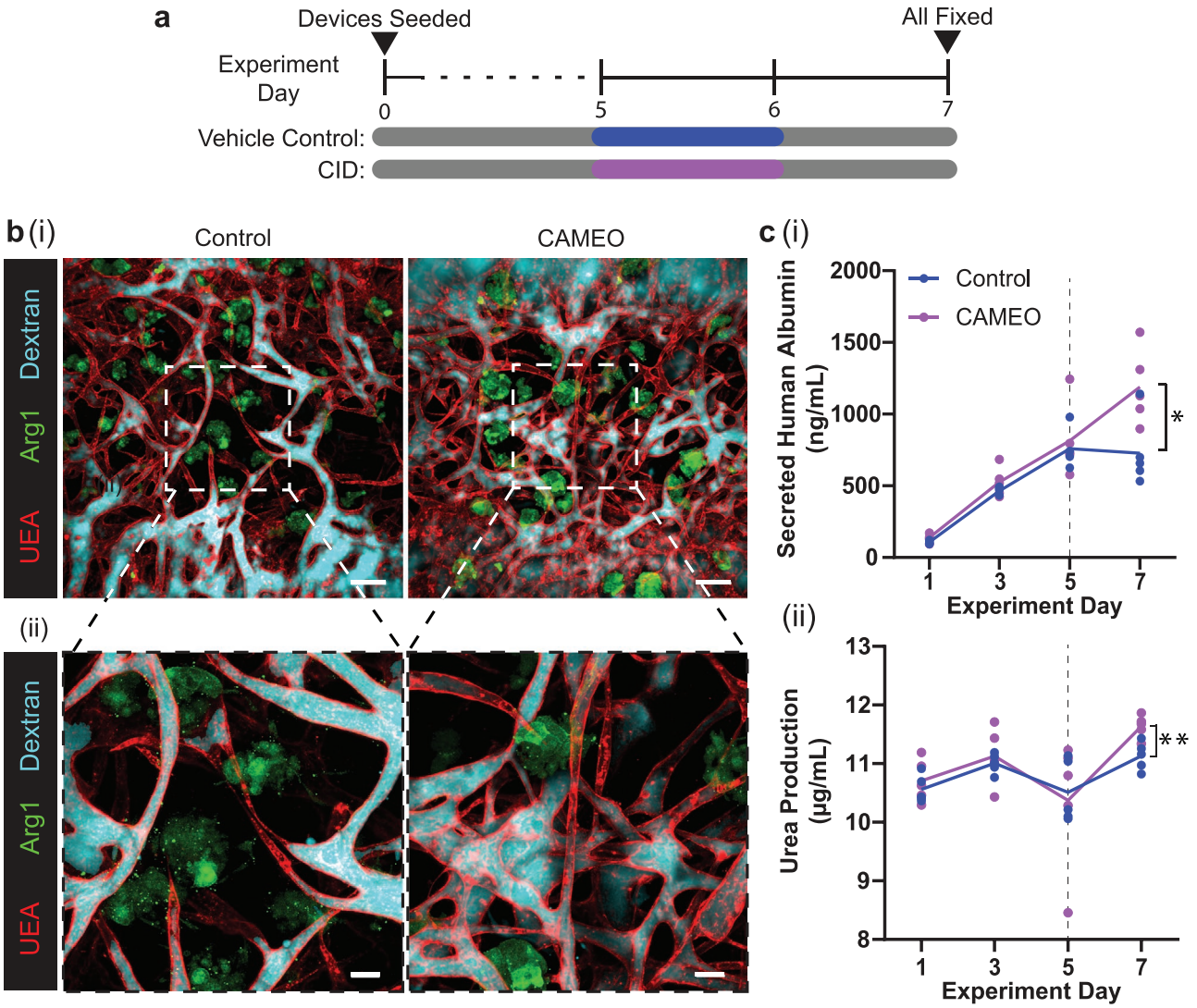

Figure 5. CAMEO enhances function of vascularized engineered hepatic tissues. a) Experimental timeline. b-i) Representative max projections of dextran-perfused (cyan) vehicle control- and CID-treated devices stained for UEA lectin (red) and human arginase 1 (green) and ii) 2.5× images. c-i) Quantification of secreted human albumin and ii) urea production in each device with mean line shown. Dotted line denotes day vehicle control and CID were dosed for 24 h. *: $p < 0.05$, **: $p < 0.01$. Scale bars: b-i) 150 µm and b-ii) 50 µm.

protein synthesis function and nitrogen metabolism, respectively, were measured in the media. Ablation of the iCasp-9 HDFs did not negatively affect the secretory functions of the hepatocytes in our devices (Figure 5c,d); in fact, we observed a statistically higher level of secreted albumin and urea at day 7 in CAMEO devices versus the vehicle control, suggesting potential benefits of removing the fibroblast population in the engineered liver constructs.

2.5. Discussion

In this study, we explored the dependence of endothelial cells on fibroblasts for forming perfusable vasculature by investigating whether a transient exposure to fibroblasts in a 3D coculture system is sufficient to drive endothelial cell morphogenesis. Whereas previous studies have shown that fibroblasts contribute to key morphogenetic steps during the formation of endothelial cell networks in vitro,[36] our study suggests that fibroblasts are only required to initiate the process of vascular network formation, which continues to develop in a semi-autonomous fashion even after fibroblasts are ablated. With CAMEO, we demonstrated that self-assembly of HUVECs into perfusable vasculature benefits from the presence of fibroblasts during the first several days of coculture, but is undisturbed when fibroblasts are ablated as early as 3 d after the coculture period. Indeed, HUVECs cultured alone formed loose networks that could not mature further into perfusable beds. While transient fibroblast coculture was sufficient to support endothelial assembly of a perfusable vascular network, additional studies will be required to fully characterize whether later stages of vascular function, such as barrier or anticoagulation functions, will require additional cell-cell interactions or will remain unaffected.

There are several known mechanisms through which stromal cells can promote vascular morphogenesis. Fibroblasts have been shown to secrete proangiogenic factors in the context of wound healing and tissue regeneration.[39–41] Nonetheless, previous studies have reported that simply transferring conditioned media from stromal cell monocultures to endothelial cells does not induce vascularization to the same extent as seen in coculture settings. Although some studies have reported success in vascularizing small (100–200 μm thickness) tissues using microfluidic systems with separate, neighboring microcompartments for endothelial cells and fibroblasts,[15,42] a study by Griffith et al. highlighted that the paracrine support of vascular morphogenesis from fibroblasts decreases dramatically with the distance between ECs and fibroblasts in separate coculture systems,[41] revealing the unique benefits of a directly mixed coculture for vascularizing larger tissues. Indeed, fibroblasts are known to actively remodel their surrounding ECM via the expression of matrix metalloproteinases (MMPs) and tissue inhibitors of metalloproteinases (TIMPs), and to deposit various ECMs such as fibronectin and collagen type III.[36,43–45] Particularly, fibronectin has been described as a provisional matrix in development and wound healing that is important for angiogenesis, vasculogenesis, and vascular remodeling.[46–48] With siRNA knockdown, we demonstrated that the initial fibronectin deposition from fibroblasts to the coculture matrix is critical for HUVECs to further develop perfusable vascular networks after the ablation of fibroblasts. This suggests that ECM deposition by the fibroblasts in the early days of coculture may be a critical cue that primes endothelial cells to continue the later stages of vascular morphogenesis without further support from fibroblasts.

Recent advancements in the tissue engineering field have enabled various types of tissues and organoids to be engineered, including brain, kidney, heart, and liver.[23,24,49–51] A main challenge in the field remains in appropriately vascularizing these tissues.[41] While using fibroblast-endothelial cell coculture methods can contribute to addressing this challenge, fibroblasts are a population of highly heterogeneous, uncharacterized cells that could potentially introduce undesirable effects such as tissue contraction, stiffening, and fibrosis.[52–56] Therefore, a vascular engineering technique that relies minimally on these cells may be desirable for clinical translation. Here, we were able to demonstrate the use of CAMEO in generating engineered liver constructs featuring dense, perfusable vasculature and a minimal population of fibroblasts. Notably, the tissues with the fibroblasts ablated at day 5 using CAMEO seemed to have enhanced secretory functions of the human primary hepatocytes compared to tissues with intact fibroblasts at day 7, highlighting unexpected potential benefits of our CAMEO platform. There are many factors that might have contributed to the improved hepatocyte function following fibroblast ablation. First, improved hepatocyte function may have been a result of reduced tissue-stiffening following fibroblast ablation, consistent with other reports that lower matrix stiffness improves primary hepatocyte function.[57–60] Second, it has been previously shown that the interaction between endothelial cells and hepatocytes can promote hepatocyte function, maintenance, and regeneration.[61–64] Ablating the fibroblasts from the hepatocyte-HUVEC-HDF tri-culture system could enhance hepatocyte-HUVEC interactions, resulting in increased albumin and urea biosynthesis. Lastly, the high density of fibroblasts in nonablated cultures may compete with hepatocytes for nutrients. Regardless, CAMEO may prove to be a useful strategy to optimize coculture conditions for engineered tissues.

Previously, inducible apoptosis transgenes like iCasp9 were developed and primarily only used as a "fail-safe" for cell-based therapies involving T-cells,[27] MSCs,[65] and stem cells.[66] In this study, we repurposed this suicide transgene and demonstrated its utility for studying cell–cell interactions as well as the subsequent impact on the functional vascularization of engineered tissues. CAMEO may offer general utility in applications beyond those demonstrated here. CAMEO could be used in culture settings, for example to eliminate xenogenic feeder-layer fibroblasts that are still widely used to cultivate embryonic, induced, and hematopoietic stem cells.[67] In tissue engineering, it may be useful to eliminate not only stromal populations, but also other cell populations that might have only a transient utility as well. Despite the enormous potential of this approach, further investigation of the induced apoptosis process and the clearing of apoptotic bodies will be needed to accurately evaluate the clinical translatability of CAMEO.

3. Conclusion

In summary, the CAMEO platform enabled by the synthetic kill-switch transgene, iCasp9, allowed for on-demand control over the specific ablation of fibroblasts in our endothelial cell-fibroblast vasculogenesis model. Using this system, we demonstrated that only a transient coculture with fibroblasts is sufficient for the endothelial cells to carry on and complete functional vascular morphogenesis, and then used these insights to generate functionally vascularized liver tissues with a minimal fibroblast population and improved secretory functions. This approach of "engineering-via-elimination" provides not only new opportunities for studying and engineering vasculature for a variety of applications, but more generally, a means to incorporate cell populations into settings where they may have only transient utility.

4. Experimental Section

Cell Preparation: HUVECs (pooled from four donors, Lonza) were cultured in Endothelial Growth Medium-2 (EGM-2, Lonza) and used before P7. HDFs (single donor; Lonza) were cultured in Fibroblast Growth Medium-2 (FGM-2, Lonza) and used before P10. Hepatic aggregates were cultured as described previously.[23,68] Briefly, cryopreserved primary human hepatocytes (Lot ZGF; BioreclamationIVT) were thawed and immediately plated with iCasp9-HDFs in a 1:1 ratio in AggreWells (400 μm pyramidal microwells) and cultured for 3 d in maintenance media containing 10% (v/v) fetal bovine serum (FBS) (Gibco), 1% (v/v) ITS supplement (insulin, transferrin, sodium selenite; BD Biosciences), glucagon (70 ng mL^{-1}), dexamethasone (0.04 μg mL^{-1}), 0.015 M HEPES, and 1% (v/v) penicillin-streptomycin (Invitrogen) in DMEM with 4.5 g L^{-1} glucose (Corning Cellgro).

Lentiviral Transduction: iCasp9-HDFs and LifeAct-Ruby-HUVECs were generated using pMSCV-F-del Casp9.IRES.GFP (gift from David Spencer, Addgene plasmid #15567) and pLenti.PGK.LifeAct-Ruby.W (gift from Rusty Landsford, Addgene plasmid #51009), respectively. Briefly, individual plasmids were cotransfected into HEK-293T cells with pVSVG,

pRSV-REV, and pMDLg/pRRE using the calcium phosphate transfection method. Supernatants containing the assembled viruses were collected after 48 h and precipitated using PEG-IT (SBI). The concentrated viral pellet was resuspended in phosphate buffer saline (PBS) and stored in −80 °C. HDFs and HUVECs were transduced in growth media overnight with the appropriate lentiviral titers that had been optimized for minimal changes in cell morphology and proliferation. The cells were then washed in PBS the next day and fed with fresh growth media for expansion. For iCasp9-HDFs, GFP+ population (top 30%) was selected via flow-assisted cytometry (FACSMelody, BD Biosciences) where the samples were first gated to exclude debris and cell doublets.

Device Assembly and Cell Seeding: The molds for the 2-channel microfluidic devices (2 cm × 1 cm × 0.3 cm) were constructed using stereolithography (Proto Labs). PDMS was cured at a standard mixing ratio overnight at 60 °C in the mold, and individual devices were cut and plasma-bonded to glass slides. To enhance ECM bonding to PDMS, the surface inside the tissue chamber of the devices was functionalized with 0.01% poly-L-lysine and 1% glutaraldehyde following plasma-activation and washed overnight in DI water. On the day of seeding, devices were soaked in 70% ethanol (EtOH) and dried. Acupuncture needles (300 µm diameter) (Hwato) were blocked in 0.1% (w/v) bovine serum albumin (BSA) (Sigma) in PBS for 45 min and inserted through the two needle guides. Devices with needles were UV-sterilized for 15 min.

On the day of device seeding, HDFs or iCasp-9 HDFs were growth-arrested with 10 µg mL^{-1} mitomycin C in FGM-2 for 2.5 h and thoroughly washed five times in fibroblast basal medium (FBM, Lonza), in order to prevent the small population of HDFs (≈4%) that remain after CID treatment from proliferating and repopulating the coculture. It was noted that mitomycin C-arrested and untreated HDFs performed similarly in their ability to support vascular morphogenesis, and the growth-arrested HDFs were used for this study. Both HUVECs and HDFs were lifted from culture plates using TrypLE Express (Gibco), centrifuged at 200 g for 4 min, and resuspended to a concentration of 20 million cells mL^{-1} in EGM-2. A solution of HUVECs (3 million cells mL^{-1}), HDFs or iCasp-9 HDFs (0, 1 million, 3 million, or 6 million cells mL^{-1}), fibrinogen (2.5 mg mL^{-1}), thrombin (1 U mL^{-1}) in EGM-2 was prepared for the bulk hydrogel region of each device. For the devices with hepatocytes, a solution of HUVECs (3 million cells mL^{-1}), iCasp-9 HDFs (total of 6 million cells mL^{-1}), hepatic aggregates (0.36 million aggregates mL^{-1} with about 150 hepatocytes per aggregate), fibrinogen (2.5 mg mL^{-1}), thrombin (1 U mL^{-1}) was made in a 1:1 media mixture of EGM-2 and hepatocyte maintenance media. After the addition of thrombin, the solution was quickly injected into the tissue chamber, and the devices were repeatedly rotated while the solution cross-linked. Appropriate media was added to each well of the device, and the devices were placed in the incubator (37 °C, 5% CO_2). After 15 min, the needles were carefully ablated from the devices to create 300 µm hollow channels between the wells. Each channel of the device was seeded with additional HUVECs at 2 million cells mL^{-1} for at least 5 min on each side (top and bottom) in the incubator. Each device received 200 µL of appropriate media daily and cultured on the rocker inside the incubator.

Vessel Network Analysis: All devices were fixed with 4% PFA for 30 min on a rocker and washed with PBS overnight at 4 °C. The devices were then blocked in 3% BSA overnight at 4 °C. Lectin (UEA DyLight 649, Vector Labs) was diluted in the blocking solution at 1:100 and added to the devices for another 4 °C overnight incubation. Devices were then washed overnight with PBS at 4 °C and kept in PBS with 0.02% (w/v) sodium azide at 4 °C until imaging.

Before imaging, a solution of 500 kDa fluorescein isothiocyanate (FITC)- or tetramethylrhodamine isothiocyanate (TRITC)-conjugated dextran (0.15 mg mL^{-1}) was added to one of the microfluidic channels to generate a pressure gradient between the two channels of the device. All device images were then captured by a Leica SP8 confocal microscope (Leica, Wetzlar, Germany) using either a Leica 10×/0.30NA W U-V-I WD-3.60 Water or 25×/0.95NA W VISIR WD-2.50 Water objective and Leica LAS X imaging software. Within experimental runs, the same laser intensities and settings were applied to all samples.

A custom MATLAB script was used to study properties of the vascular network (refer to Supporting Information for the code). The script imports a .tif image stack with a surface marker in one channel, in this case lectin, and the fluorescent dye in another, FITC- or TRITC-dextran. The aspect ratio of each image was adjusted so that each voxel was equally sized in all directions. Since the image resolution was higher in-plane (*x*- and *y*-axes) than along the depth (*z*-axis), this step typically resulted in a reduction in the number of pixels in the plane and an increase in the number of stack layers. The 3D volume of the cell surface marker channel was then smoothed using a spatial-domain Gaussian kernel to reduce noise in the Lectin channel.

The script relies on user inputs to generate binary images of the complete vascular network from the Lectin signal, and the perfused network according to the FITC-Dextran. First, the user selects a 2D region of interest between the two needle-molded channels on the device, and performs contrast-limited adaptive histogram equalization (CLAHE) on both signals for each *z* slice.[69] This step was performed to overcome a substantial loss in signal with depth of the volume.

The user then specifies a luminance threshold for each channel and is able to move between different images in the *z* stack to best capture the vessel structure and perfusion of FITC-Dextran. For the fluorescent dye, the signal was processed using only this specified uniform threshold to capture the regions of perfusion. For the Lectin channel, which exhibits poorer contrast, the user first selects a liberal threshold to segment the 3D volume. The script refines this initial segmentation for each slice using distance regularized level set evolution (DRLSE) with a double well potential (see full code for setup of the iterative segmentation refinement).[70] The DRLSE-segmented slices were merged to form the final volume of the full vessel network. Any holes in the Lectin volume were filled and islands smaller than ≈50 µm^3 were removed.

From the identified Lectin network, a 3D medial axis skeleton was generated using homotopic thinning.[71,72] This was further converted into a graph with links representing the vessel structures, and nodes to identify branching and terminal points of the vessels.[72] Links were further characterized as perfused and nonperfused vessels based on the overlap of the binarized FITC-Dextran with the vessel network. Links with <25% perfusion were classified as nonperfused links. The average length of all links from the Lectin skeleton was reported. The vessel radii were calculated based on the distance between the surface and the medial skeleton of the graph links, and the mean diameters for all vessels, as well as only perfused vessels, were reported. The percentages reported for branching nodes represented the fraction of branching nodes out of all nodes. The user could toggle through the *z*-stack of the binary channels overlaid on the original images, as well as overlaid on each other to confirm accuracy.

Viability and Inflammation Assays: For the ATP assay, iCasp9-HDFs were plated in monolayer (8500 cells per well in a 96-well plate). On the next day, cultures were dosed with CID (B/B homodimerizer aka AP20187) (Takara) at concentrations of 5×10^{-9}, 50×10^{-9}, or 500×10^{-9} M and assayed for ATP levels using the CellTiter-Glo Luminescent Cell Viability Assay (Promega) according to the manufacturer's instructions. For the cell-counting assay, iCasp9-HDFs were first mitomycin-treated for 2.5 h at 10 µg mL^{-1} and washed three times with FBM. Then, the cells were plated at 60 000 cells per well in 24-well plates and cultured overnight in the incubator. On the next day, the wells were treated with either 10×10^{-9} M CID or ethanol vehicle and cultured overnight in the incubator. These wells were then fixed with 4% PFA, washed with PBS, stained with DAPI (1:1000) (Sigma), and stored at 4 °C. The nuclei of the cells were imaged with a Nikon TE 200 microscope with a Nikon 20×/0.50NA objective and Spot Imaging 5.3 software. Cell nuclei were counted using CellProfiler to compare cell counts between vehicle and CID treatment.[73] For visualization of the cell bodies, some wells were stained with Alexa Fluor 568 Phalloidin (1:200) (Life Technologies) and imaged with a Leica SP8 confocal microscope (Leica, Wetzlar, Germany) using a Leica 25×/0.95NA W VISIR WD-2.50 Water objective and Leica LAS X imaging software.

For the inflammation assay, 16-well chamber slides (Lab-Tek) were first coated with human fibronectin (Corning) at 10 µg mL^{-1}. For CID and vehicle conditions, each well was seeded with 7000 HUVECs and 14 000 iCasp9-HDFs in EGM-2 media, and the cells were allowed to

attach and spread overnight. On the next day, the wells were treated with fresh EGM-2 media containing either CID (10×10^{-9} M) or vehicle. For the positive control condition, 7000 HUVECs were added in each well in EGM-2 media, and on the next day, the wells were seeded with fresh EGM-2 media containing human recombinant TNF-α (R&D Systems) at 10 ng mL^{-1}. In all conditions, cells were fixed at 4, 12, 24, or 48 h post-treatment with 4% PFA. No media was changed between treatment and fixation. The fixed samples were permeabilized with 0.25% Triton X-100 for 10 min and blocked with 3% BSA for 1 h at room temperature. The samples were then stained with rabbit NFκB primary antibody (1:500) (Cell Signaling, D14E12) and UEA lectin (1:500) for 1 h at room temperature, followed by secondary goat antirabbit Alexa Fluor 568 (1:1000) and DAPI (1:1000) staining overnight at 4C. Samples were stored in PBS at 4C until imaging. Samples were imaged by a Leica SP8 confocal microscope (Leica, Wetzlar, Germany) using a 25×/0.95NA W VISIR WD-2.50 Water objective and Leica LAS X imaging software. The percentage of endothelial cells with nuclear NFκB was calculated by manually counting the total number of UEA-positive endothelial cells and the number of UEA-positive and nuclear NFκB-positive endothelial cells.

Culture Live Imaging: Microfluidic devices with LifeAct-Ruby HUVECs and iCasp9-HDFs (GFP) were made and cultured for 7 d as described above. Then, the devices were transferred to a custom-made Petri dish that limits media evaporation. Media was changed to EGM-2 containing OxyFluor (Oxyrase) at a 1:100 dilution. Right before the start of imaging, either CID (10×10^{-9} M) or vehicle was added to the devices and the petri dish was transferred into the microscope environmental chamber preconditioned to 37 °C, 5% CO2, and 100% humidity. A 150 µm stack was imaged in each device by a Yokogawa CSU-10/Zeiss Axiovert 200M inverted spinning-disk microscope using a Zeiss 10×/0.45NA Air objective every 30 min for 18 h. The capture was automated using Metamorph 7.8.9.0 (Molecular Devices).

Nanoindentation Characterization: Acellular fibrin gels and fibrin gels with HUVECs and iCasp9-HDF at 3:6 HUVEC:HDF ratio were prepared as described above in 2 mm diameter PDMS wells. Nanoindentation characterization was performed using a Piuma Nanoindenter system (Optics 11, Westwood, MA). The spherical indentation probe had a diameter size ≈100 µm with cantilever spring constant k ≈ 0.5 N m^{-1}. Samples were immersed in EGM2 medium and measurements were performed at indentation depth of 10 µm and displacement speed of 5 µm s^{-1} with 4–5 repeats for each condition. The Young's moduli of these samples were calculated using the built-in Piuma software by fitting force-indentation curves to the Hertzian contact mechanics model, assuming a Poisson ratio of 0.5 for incompressible materials. Optics11 DataViewer software was used for data analysis. Acellular fibrin gels were measured at day 3 and tissues with HUVECs and iCasp9-HDFs were measured at day 3, 4, or 7. For the tissues measured at day 4 or day 7, CID (10×10^{-9} M) or vehicle was added to the media at day 3.

Coculture with Fibronectin Knockdown Fibroblasts: iCasp9-HDFs were plated in 35 mm dishes and allowed to expand to ≈50% confluence. On the morning of transfection, media was replaced with an antibiotic-free media. At the end of the day, dishes were transfected with 20×10^{-12} M of either human FN1 siRNA or human scrambled siRNA in a SMARTpool format (Dharmacon). siRNA was diluted in OPTI-MEM (Gibco) media and mixed with Lipofectamine RNAiMAX (Invitrogen) in OPTI-MEM. Mixtures were incubated at room temperature for 5 min, after which they were added dropwise to the cell dishes and incubated for 24 h. On the next day, the cells were washed with FBM five times. Microfluidic devices with HUVECs and iCasp9-HDFs (treated with fibronectin or scramble siRNA) in fibrin were prepared as described above at 3:6 HUVEC:HDF ratio and cultured for 7 d in EGM-2. At day 3, all the devices were treated with 10×10^{-9} M of CID. Devices were fixed at day 7 and imaged for vessel network analysis as described above.

Hepatocyte Functional Assays: On days 1, 3, 5, and 7, cultured media from the devices was collected and stored at −80 °C. Supernatant was thawed to room temperature and assayed for human albumin using an enzyme-linked immunosorbent assay (ELISA) (Bethyl Laboratories) and 3,3',5,5'-tetramethylbenzidine (TMB, Thermo Fisher), as well as urea using a colorimetric (diacetylmonoxime) assay with acid and heat (Stanbio Labs).

All triculture devices were fixed with 4% PFA for 30 min on a rocker and washed with PBS overnight at 4 °C. The devices were permeabilized with 0.15% Triton-X for 30 min on a rocker and washed with PBS 3 times. The devices were then blocked in 3% BSA overnight at 4 °C. Dylight 649 labeled UEA (Vector Laboratories) and primary antibody for rabbit antihuman arginase-1 (Sigma, HPA003595) were diluted in the blocking solution at 1:200 and 1:100 respectively and added to the devices overnight at 4 °C. The devices were washed with PBS overnight at 4 °C. Goat antirabbit Alexa Fluor 568 secondary antibody was diluted in the blocking solution at 1:100 and added to the devices overnight at 4 °C. Devices were then washed overnight with PBS overnight at 4 °C and kept in PBS with 0.02% (w/v) sodium azide at 4 °C until imaging. A FITC-conjugated 500 kDa dextran solution (1.5 mg mL^{-1}) was added to the devices as described above right before imaging. All device images were then captured by a Leica SP8 confocal microscope (Leica, Wetzlar, Germany) using either a Leica 10×/0.30NA W U-V-I WD-3.60 Water or 25×/0.95NA W VISIR WD-2.50 Water objective, and Leica LAS X imaging software.

Image Processing: Max projection images used in figures were assembled and processed using Imaris 9.2.1 (Bitplane). Intensity of stack images was depth compensated by utilizing a built-in autocorrelation correction Matlab plug-in (MathWorks). The dextran channels were smoothed using the Gaussian Filter that used a 3.89 µm filter width in order to make perfused channels more clearly visible in figures (Figure S5, Supporting Information). Thresholding and gamma correction were applied to all images. Both the UEA lectin and TRITC- Dextran were false-colored to red and cyan, respectively. Only unprocessed images were used in the image analysis, explained above. For images containing hepatocytes, false coloring was applied to UEA lectin, FITC Dextran and Arg1 as red, cyan, and green, respectively. Uniform volumetric masks were applied that were thresholded to denoise images due to antibody aggregation and fluorophore bleed through. These corrections were applied to the Dextran and Arg1 channels in all hepatocyte images.

Statistical Analysis: All data were presented as mean ± standard deviation. At least three independent samples were analyzed for quantified sections. All statistical significance was determined using Prism (GraphPad, San Diego, CA). CID-induced cell count reduction in 2D was quantified by a two-tailed Welch's *t*-test. Hepatocyte function data (albumin and urea), vascular network metrics for FN-KD experiments, and nanoindentation results were analyzed by unpaired two-tailed *t*-tests. All other mean analyses were performed using ordinary one-way ANOVA and, where appropriate, followed by Tukey's honest significance test to evaluate statistical significance ($p < 0.05$).

Supporting Information

Supporting Information is available from the Wiley Online Library or from the author.

Acknowledgements

The authors thank Wilson Wong for guidance and helpful discussions regarding iCasp9 constructs. This work was supported in part by grants from the National Institutes of Health (EB00262, EB08396, and UG3 EB017103), the National Science Foundation Cellular Metamaterials Engineering Research Center, the Boston University Biological Design Center, and Koch Institute Support (core) Grant P30-CA14051 from the National Cancer Institute. A.L. acknowledges financial support from the NIH T32 Quantitative Biology and Physiology training grant and S.S. was supported by the American Heart Association Postdoctoral Fellowship. A.X.C. was supported by the National Science Foundation Graduate Research Fellowship (1122374). S.N.B.is a Howard Hughes Medical Institute Investigator.

Conflict of Interest

S.N.B. is a director at Vertex, cofounder and consultant at Glympse Bio, consultant for Cristal, Maverick, and Moderna, and receives sponsored research funding from Johnson & Johnson.

Keywords

fibroblasts, neovascularization, organ engineering, vascular engineering, vasculogenesis

Received: April 30, 2020
Revised: May 26, 2020
Published online: June 25, 2020

[1] M. Potente, H. Gerhardt, P. Carmeliet, *Cell* **2011**, *146*, 873.
[2] A. Luttun, P. Carmeliet, *Stem Cells: From Basic Research to Therapy*, Vol. *2*, CRC Press, Boca Raton, FL **2014**, p. 104.
[3] S. P. Herbert, D. Y. R. Stainier, *Nat. Rev. Mol. Cell Biol.* **2011**, *12*, 551.
[4] M. A. Traore, S. C. George, *Tissue Eng., Part B* **2017**, *23*, 505.
[5] H. H. G. Song, R. T. Rumma, C. K. Ozaki, E. R. Edelman, C. S. Chen, *Cell Stem Cell* **2018**, *22*, 340.
[6] G. E. Davis, C. W. Camarillo, *Exp. Cell Res.* **1996**, *224*, 39.
[7] W. B. Saunders, B. L. Bohnsack, J. B. Faske, N. J. Anthis, K. J. Bayless, K. K. Hirschi, G. E. Davis, *J. Cell Biol.* **2006**, *175*, 179.
[8] D. M. Barry, Y. Koo, P. R. Norden, L. A. Wylie, K. Xu, C. Wichaidit, D. B. Azizoglu, Y. Zheng, M. H. Cobb, G. E. Davis, O. Cleaver, *Circ. Res.* **2016**, *119*, 810.
[9] W. Koh, R. D. Mahan, G. E. Davis, *J. Cell Sci.* **2008**, *121*, 989.
[10] A. N. Stratman, G. E. Davis, *Microsc. Microanal.* **2012**, *18*, 68.
[11] M. Kamei, W. Brian Saunders, K. J. Bayless, L. Dye, G. E. Davis, B. M. Weinstein, *Nature* **2006**, *442*, 453.
[12] J. W. Song, L. L. Munn, *Proc. Natl. Acad. Sci. USA* **2011**, *108*, 15342.
[13] P. A. Galie, D.-H. T. Nguyen, C. K. Choi, D. M. Cohen, P. A. Janmey, C. S. Chen, *Proc. Natl. Acad. Sci. USA* **2014**, *111*, 7968.
[14] L. F. Alonzo, M. L. Moya, V. S. Shirure, S. C. George, *Lab Chip* **2015**, *15*, 3521.
[15] S. Kim, H. Lee, M. Chung, N. L. Jeon, *Lab Chip* **2013**, *13*, 1489.
[16] Y.-H. Hsu, M. L. Moya, P. Abiri, C. C. W. Hughes, S. C. George, A. P. Lee, *Lab Chip* **2013**, *13*, 81.
[17] G. Cheng, S. Liao, H. K. Wong, D. A. Lacorre, E. Di Tomaso, P. Au, D. Fukumura, R. K. Jain, L. L. Munn, *Blood* **2011**, *118*, 4740.
[18] R. Samuel, L. Daheron, S. Liao, T. Vardam, W. S. Kamoun, A. Batista, C. Buecker, R. Schäfer, X. Han, P. Au, D. T. Scadden, D. G. Duda, D. Fukumura, R. K. Jain, *Proc. Natl. Acad. Sci. USA* **2013**, *110*, 12774.
[19] X. Chen, A. S. Aledia, S. A. Popson, L. Him, C. C. W. Hughes, S. C. George, *Tissue Eng., Part A* **2010**, *16*, 585.
[20] S. Levenberg, J. Rouwkema, M. Macdonald, E. S. Garfein, D. S. Kohane, D. C. Darland, R. Marini, C. A. van Blitterswijk, R. C. Mulligan, P. A. D'Amore, R. Langer, *Nat. Biotechnol.* **2005**, *23*, 879.
[21] S. Levenberg, J. S. Golub, M. Amit, J. Itskovitz-Eldor, R. Langer, *Proc. Natl. Acad. Sci. USA* **2002**, *99*, 4391.
[22] H. E. Abaci, Z. Guo, A. Coffman, B. Gillette, W. H. Lee, S. K. Sia, A. M. Christiano, *Adv. Healthcare Mater.* **2016**, *5*, 1800.
[23] K. R. Stevens, M. A. Scull, V. Ramanan, C. L. Fortin, R. R. Chaturvedi, K. A. Knouse, J. W. Xiao, C. Fung, T. Mirabella, A. X. Chen, M. G. McCue, M. T. Yang, H. E. Fleming, K. Chung, Y. P. de Jong, C. S. Chen, C. M. Rice, S. N. Bhatia, *Sci. Transl. Med.* **2017**, *9*, eaah5505.
[24] K. Ronaldson-Bouchard, S. P. Ma, K. Yeager, T. Chen, L. Song, D. Sirabella, K. Morikawa, D. Teles, M. Yazawa, G. Vunjak-Novakovic, *Nature* **2018**, *556*, 239.
[25] J. T. Hinson, A. Chopra, N. Nafissi, W. J. Polacheck, C. C. Benson, S. Swist, J. Gorham, L. Yang, S. Schafer, C. C. Sheng, A. Haghighi, J. Homsy, N. Hubner, G. Church, S. A. Cook, W. A. Linke, C. S. Chen, J. G. Seidman, C. E. Seidman, *Science* **2015**, *349*, 982.
[26] S.-K. Tey, G. Dotti, C. M. Rooney, H. E. Heslop, M. K. Brenner, *Biol. Blood Marrow Transplant.* **2007**, *13*, 913.
[27] A. Di Stasi, S.-K. Tey, G. Dotti, Y. Fujita, A. Kennedy-Nasser, C. Martinez, K. Straathof, E. Liu, A. G. Durett, B. Grilley, H. Liu, C. R. Cruz, B. Savoldo, A. P. Gee, J. Schindler, R. A. Krance, H. E. Heslop, D. M. Spencer, C. M. Rooney, M. K. Brenner, *N. Engl. J. Med.* **2011**, *365*, 1673.
[28] K. C. Straathof, M. A. Pulè, P. Yotnda, G. Dotti, E. F. Vanin, M. K. Brenner, H. E. Heslop, D. M. Spencer, C. M. Rooney, *Blood* **2005**, *105*, 4247.
[29] D.-H. T. Nguyen, S. C. Stapleton, M. T. Yang, S. S. Cha, C. K. Choi, P. A. Galie, C. S. Chen, *Proc. Natl. Acad. Sci. USA* **2013**, *110*, 6712.
[30] B. Trappmann, B. M. Baker, W. J. Polacheck, C. K. Choi, J. A. Burdick, C. S. Chen, *Nat. Commun.* **2017**, *8*, 371.
[31] P. Ramalingam, M. G. Poulos, E. Lazzari, M. C. Gutkin, D. Lopez, C. C. Kloss, M. J. Crowley, L. Katsnelson, A. G. Freire, M. B. Greenblatt, C. Y. Park, J. M. Butler, *Nat. Commun.* **2020**, *11*, 666.
[32] J. S. Pober, W. C. Sessa, *Nat. Rev. Immunol.* **2007**, *7*, 803.
[33] L. Xiao, Y. Liu, N. Wang, *Am. J. Physiol.: Heart Circ. Physiol.* **2014**, *306*, H317.
[34] D. R. Croft, M. L. Coleman, S. Li, D. Robertson, T. Sullivan, C. L. Stewart, M. F. Olson, *J. Cell Biol.* **2005**, *168*, 245.
[35] G. R. Wickman, L. Julian, K. Mardilovich, S. Schumacher, J. Munro, N. Rath, S. Al Zander, A. Mleczak, D. Sumpton, N. Morrice, W. V. Bienvenut, M. F. Olson, *Cell Death Differ.* **2013**, *20*, 1293.
[36] A. C. Newman, M. N. Nakatsu, W. Chou, P. D. Gershon, C. C. W. Hughes, *Mol. Biol. Cell* **2011**, *22*, 3791.
[37] A. C. Newman, W. Chou, K. M. Welch-Reardon, A. H. Fong, S. A. Popson, D. T. Phan, D. R. Sandoval, D. P. Nguyen, P. D. Gershon, C. C. W. Hughes, *Arterioscler., Thromb., Vasc. Biol.* **2013**, *33*, 513.
[38] X. Zhou, R. G. Rowe, N. Hiraoka, J. P. George, D. Wirtz, D. F. Mosher, I. Virtanen, M. A. Chernousov, S. J. Weiss, *Genes Dev.* **2008**, *22*, 1231.
[39] L. A. DiPietro, *J. Leukocyte Biol.* **2016**, *100*, 979.
[40] Y. Xiao, C. Liu, Z. Chen, M. R. Blatchley, D. Kim, J. Zhou, M. Xu, S. Gerecht, R. Fan, *Adv. Biosyst.* **2019**, *3*, 1900089.
[41] C. K. Griffith, C. Miller, R. C. A. Sainson, J. W. Calvert, N. L. Jeon, C. C. W. Hughes, S. C. George, *Tissue Eng.* **2005**, *11*, 257.
[42] J. A. Whisler, M. B. Chen, R. D. Kamm, *Tissue Eng., Part C* **2014**, *20*, 543.
[43] A. Orimo, P. B. Gupta, D. C. Sgroi, F. Arenzana-Seisdedos, T. Delaunay, R. Naeem, V. J. Carey, A. L. Richardson, R. A. Weinberg, *Cell* **2005**, *121*, 335.
[44] R. Costa-Almeida, R. Soares, P. L. Granja, *J. Tissue Eng. Regener. Med.* **2018**, *12*, 240.
[45] C. C. W. Hughes, *Curr. Opin. Hematol.* **2008**, *15*, 204.
[46] R. A. F. Clark, P. DellaPelle, E. Manseau, J. M. Lanigan, H. F. Dvorak, R. B. Colvin, *J. Invest. Dermatol.* **1982**, *79*, 269.
[47] A. Van Der Flier, K. Badu-Nkansah, C. A. Whittaker, D. Crowley, R. T. Bronson, A. Lacy-Hulbert, R. O. Hynes, *Development* **2010**, *137*, 2439.
[48] H. Y. Chiang, V. A. Korshunov, A. Serour, F. Shi, J. Sottile, *Arterioscler., Thromb., Vasc. Biol.* **2009**, *29*, 1074.
[49] M. A. Lancaster, N. S. Corsini, S. Wolfinger, E. H. Gustafson, A. W. Phillips, T. R. Burkard, T. Otani, F. J. Livesey, J. A. Knoblich, *Nat. Biotechnol.* **2017**, *35*, 659.
[50] K. A. Homan, N. Gupta, K. T. Kroll, D. B. Kolesky, M. Skylar-Scott, T. Miyoshi, D. Mau, M. T. Valerius, T. Ferrante, J. V. Bonventre, J. A. Lewis, R. Morizane, *Nat. Methods* **2019**, *16*, 255.
[51] H. Clevers, *Cell* **2016**, *165*, 1586.

[52] C. D. Buckley, D. Pilling, J. M. Lord, A. N. Akbar, D. Scheel-Toellner, M. Salmon, *Trends Immunol.* **2001**, *22*, 199.
[53] T. A. Wynn, T. R. Ramalingam, *Nat. Med.* **2012**, *18*, 1028.
[54] J. S. Jeon, S. Bersini, J. A. Whisler, M. B. Chen, G. Dubini, J. L. Charest, M. Moretti, R. D. Kamm, *Integr. Biol.* **2012**, *100*, 130.
[55] V. S. LeBleu, G. Taduri, J. O'Connell, Y. Teng, V. G. Cooke, C. Woda, H. Sugimoto, R. Kalluri, *Nat. Med.* **2013**, *19*, 1047.
[56] D. R. Lemos, J. S. Duffield, *Sci. Transl. Med.* **2018**, *10*, eaan5174.
[57] S. S. Desai, J. C. Tung, V. X. Zhou, J. P. Grenert, Y. Malato, M. Rezvani, R. Español-Suñer, H. Willenbring, V. M. Weaver, T. T. Chang, *Hepatology* **2016**, *64*, 261.
[58] T. Xia, R. Zhao, W. Liu, Q. Huang, P. Chen, Y. N. Waju, M. K. Al-ani, Y. Lv, L. Yang, *J. Cell. Physiol.* **2018**, *233*, 6996.
[59] V. Natarajan, E. J. Berglund, D. X. Chen, S. Kidambi, *RSC Adv.* **2015**, *5*, 80956.
[60] P. Godoy, J. G. Hengstler, I. Ilkavets, C. Meyer, A. Bachmann, A. Müller, G. Tuschl, S. O. Mueller, S. Dooley, *Hepatology* **2009**, *49*, 2031.
[61] C. Géraud, P. S. Koch, J. Zierow, K. Klapproth, K. Busch, V. Olsavszky, T. Leibing, A. Demory, F. Ulbrich, M. Diett, S. Singh, C. Sticht, K. Breitkopf-Heinlein, K. Richter, S. M. Karppinen, T. Pihlajaniemi, B. Arnold, H. R. Rodewald, H. G. Augustin, K. Schledzewski, S. Goerdt, *J. Clin. Invest.* **2017**, *127*, 1099.
[62] L. D. DeLeve, *J. Clin. Invest.* **2013**, *123*, 1861.
[63] Y. Manavski, T. Abel, J. Hu, D. Kleinlützum, C. J. Buchholz, C. Belz, H. G. Augustin, R. A. Boon, S. Dimmeler, *Proc. Natl. Acad. Sci. USA* **2017**, *114*, 3993.
[64] B.-S. Ding, D. J. Nolan, J. M. Butler, D. James, A. O. Babazadeh, Z. Rosenwaks, V. Mittal, H. Kobayashi, K. Shido, D. Lyden, T. N. Sato, S. Y. Rabbany, S. Rafii, *Nature* **2010**, *468*, 310.
[65] F. Rossignoli, G. Grisendi, C. Spano, G. Golinelli, A. Recchia, G. Rovesti, G. Orsi, E. Veronesi, E. M. Horwitz, M. Dominici, *Cancer Gene Ther.* **2019**, *26*, 11.
[66] C. Wu, S. G. Hong, T. Winkler, D. M. Spencer, A. Jares, B. Ichwan, A. Nicolae, V. Guo, A. Larochelle, C. E. Dunbar, *Mol. Ther. – Methods Clin. Dev.* **2014**, *1*, 14053.
[67] M. Richards, C. Y. Fong, W. K. Chan, P. C. Wong, A. Bongso, *Nat. Biotechnol.* **2002**, *20*, 933.
[68] K. R. Stevens, M. D. Ungrin, R. E. Schwartz, S. Ng, B. Carvalho, K. S. Christine, R. R. Chaturvedi, C. Y. Li, P. W. Zandstra, C. S. Chen, S. N. Bhatia, *Nat. Commun.* **2013**, *4*, 1847.
[69] K. Zuiderveld, in *Graphics Gems IV* (Ed.: P. S. Heckbert), Academic Press Professional, Inc., San Diego, CA, USA **1994**, pp. 474–485.
[70] C. Li, C. Xu, C. Gui, M. D. Fox, *IEEE Trans. Image Process.* **2010**, *19*, 1371.
[71] T.-C. Lee, R. L. Kashyap, C.-N. Chu, *CVGIP Graphical Models Image Process.* **1994**, *56*, 462.
[72] P. Kollmannsberger, M. Kerschnitzki, F. Repp, W. Wagermaier, R. Weinkamer, P. Fratzl, *New J. Phys.* **2017**, *19*, 073019.
[73] C. McQuin, A. Goodman, V. Chernyshev, L. Kamentsky, B. A. Cimini, K. W. Karhohs, M. Doan, L. Ding, S. M. Rafelski, D. Thirstrup, W. Wiegraebe, S. Singh, T. Becker, J. C. Caicedo, A. E. Carpenter, *PLoS Biol.* **2018**, *16*, e2005970.